

Pulsed-laser-induced damage in rat corneas: time-resolved imaging of physical effects and acute biological response

Anoop V. Cherian

Kaustubh R. Rau

National Centre for Biological Sciences-TIFR
PO GKVK Bellary Road
Bangalore 560065, India
E-mail: kaustubh@ncbs.res.in

Abstract. Laser-induced damage is studied in the rat corneal epithelium and stroma using a combination of time-resolved imaging and biological assays. Cavitation bubble interactions with cells are visualized at a higher spatial resolution than previously reported. The shock wave is observed to propagate through the epithelium without cell displacement or deformation. Cavitation bubble expansion is damped in tissue with a reduction in maximum size in the range of 54 to 59%, as compared to 2-D and 3-D cultures. Bubble expansion on nanosecond timescales results in rupture of the epithelial sheet and severe compression of cell layers beyond the bubble rim. In the stroma, the dense collagen lamellae strongly damped bubble expansion, thus resulting in reduced damage. The acute biological response of this tissue to laser pulses is characterized by confocal fluorescence microscopy. A viability assay of the epithelium reveals that only cells around the immediate site of laser focus are killed, while cells seen to undergo large deformations remain alive. Actin morphology in cells facing this mechanical stress is unchanged. Collagen microstructure in the stroma as revealed by second-harmonic imaging around the ablation site shows minimal disruption. These cellular responses are also compared to *in vitro* 2-D and 3-D cell cultures. © 2008 Society of Photo-Optical Instrumentation Engineers. [DOI: 10.1117/1.2907214]

Keywords: laser-induced damage; ablation; time-resolved imaging; cavitation; shock wave; cornea; fluorescence microscopy.

Paper 07364RR received Sep. 4, 2007; revised manuscript received Nov. 28, 2007; accepted for publication Nov. 29, 2007; published online Apr. 21, 2008.

1 Introduction

The complexity of laser-tissue interactions has led to the continuing study of this subject since the introduction of lasers in surgery.¹ In particular, pulsed laser-tissue interactions have been the topic of detailed study due to their widespread use for tissue ablation.^{2,3} This topic has also received recent attention due to the increasing use of picosecond and femtosecond duration lasers for precise tissue ablation due to the reduced collateral damage observed with ultrafast lasers as compared to nanosecond lasers.⁴ In cell biology, laser microdissection and catapulting with UV or visible laser wavelengths for isolation of a group of cells from a tissue sample, intracellular surgery, and single-cell analysis are also finding increasing uses.⁵⁻⁸

Laser-induced plasma formation or optical breakdown is the primary mechanism of interaction when pulsed lasers are used for surgery or in cellular micromanipulation. At nanosecond pulse durations, plasma formation is initiated when the intensity of the laser beam in the focal spot crosses a critical threshold ($I_{th} > 10^{10}$ W/cm²) necessary for generation of seed-free electrons. Acoustic phenomena seen after plasma

initiation such as shock wave radiation and cavitation bubble generation have been the subject of detailed study in homogeneous media such as water or tissue phantoms such as gelatin and polyacrylamide gels.⁹⁻¹⁴ These have provided us with a clear understanding of this process and related physical parameters such as pulse energy dependencies, time scales, cavitation, and shock pressures. The dynamics of these processes have also been studied in tissue such as enucleated bovine corneas.¹⁵⁻¹⁹ In studies by Juhasz et al. time-resolved imaging was used to determine shock wave and cavitation bubble dynamics when bovine corneas were irradiated with picosecond and femtosecond duration laser pulses.^{15,16} It was seen that shock wave dynamics were similar to those in water, with shock pressures in the gigapascal range close to the irradiation site. Cavitation bubbles attained a smaller maximum size in cornea as compared to expansion in water. While these studies made it possible to quantify the cavitation dynamics, the low spatial resolution did not allow visualization of the cavitation bubble-cell interactions, and thus their impact on cellular damage could not be ascertained. Extensive studies by Vogel et al. have also provided a clear exposition of the damage process in tissue and the contributions of the individual mechanical processes such as cavitation bubble collapse and jet

Address all correspondence to Kaustubh Rau, National Centre for Biological Sciences, GKVK Campus, Bellary Road - Bangalore, Karnataka 560065, India; Tel: 91-80-23636220; Fax: 91-80-23636662; E-mail: kaustubh@ncbs.res.in

formation to it.¹⁷⁻¹⁹ In a number of studies on the impact of laser pulses (nanosecond to picosecond in pulse duration) in *ex vivo* corneas, time-resolved imaging was used to examine the bubble dynamics.¹⁸ These images showed that similar to the Juhasz et al. studies, cavitation bubbles attained a smaller maximum size due to the collagen organization in the stroma. The tissue morphology was examined by histology and secondary electron microscopy providing information on large-scale damage effects of cavitation forces such as jet impact and shear flow.¹⁷ Studies by other groups on the effects of femtosecond laser pulses in tissue by using histopathology and scanning electron microscopy (SEM) to determine the morphological changes after irradiation have also been reported.²⁰⁻²³ These studies were primarily conducted to determine the suitability of using ultrafast lasers for corneal refractive surgery by determining the characteristics of the ablation pattern and hence the cavitation dynamics were not studied.

Parallel to ablation studies in the cornea, researchers, have also examined the wound healing response of corneal tissue. Injury to the cornea during laser-assisted *in situ* keratomilectomy (LASIK), Photorefractive keratectomy (PRK), or femtosecond laser surgery has been determined by a variety of wound healing assays that examine the production of cytokines,²⁴ laying down of matrix proteins such as fibronectin and tenascin, and the migration of keratocytes into the wound site.²⁵ In a majority of these studies, the mechanism of damage is not due to cavitation (e.g., LASIK and PRK). Where this is the case (e.g., femtosecond laser surgery), the cavitation dynamics have not been studied and thus cannot be related to the observed biological response.^{26,27}

In this study we examined cavitation damage produced using nanosecond laser pulses at $\lambda=532$ nm in *ex vivo* samples of rat corneas. As already detailed, ablation with nanosecond laser pulses has received considerable attention. However, there have been few high-resolution investigations of cavitation bubble-cell interactions in tissue and none where the biological response to the cavitation was examined in detail. As highlighted in a recent study of laser ablation using a nanosecond source, the physical properties of tissue, specifically the elastic/plastic response, play an important role in determining damage, emphasizing the fact that complete understanding of this topic is still lacking.²⁸ Our objective thus was to conduct a basic study of tissue ablation to study the bubble dynamics and cellular response. To accomplish this, we combined time-resolved imaging to capture the cavitation dynamics in corneal tissue and confocal fluorescence microscopy to determine the biological response postirradiation. The high-spatial-resolution imaging system employed for this study visualized cellular response to cavitation in greater detail than earlier reports.^{15,16,18} Postirradiation, these tissue were examined to determine changes in cell viability, actin cytoskeleton, and collagen microstructure, enabling us to examine the microeffects of cavitation forces on cells. As control samples we also conducted ablation studies on *in vitro* 3-D and 2-D cultures. In conjunction with corneal tissue, the *in vitro* samples enabled us to determine the role of the matrix and cell organization in determining damage during cavitation. The results of our study would also be relevant to tissue ablation with picosecond or femtosecond laser pulses and provide a basis for further studies using ultrafast lasers.

2 Materials and Methods

2.1 Rat Corneas

Freshly dissected rat eyes were obtained from Wistar rats sacrificed for neurobiology experiments at our institute. The cornea was excised from the eyeball using a surgical blade and washed thrice with minimal essential medium (MEM). It was then dissected into four equal parts with one part being used for the experiment. The sample was placed in 35-mm plastic tissue culture dishes with the epithelium facing down (in contact with the coverslip), immersed in MEM and used for irradiation experiments. Viability assays on control samples indicated that epithelial cells remained viable after 6 h at room temperature.

2.2 3-D Cell Cultures

Reconstitution buffer was made with 2.2 g NaHCO_3 and 4.77 g HEPES in 100 mL, 50-mM NaOH and sterilized by passing through a 0.22- μm filter. Seven parts of rat-tail collagen Type I (BD Biosciences) were mixed with two parts of $5\times$ Dulbecco's modified Eagle's medium (DMEM) and one part of reconstitution buffer and neutralised with 1-M NaOH to pH 7.4 ± 0.2 . NIH 3T3 fibroblasts were added to this solution to a final concentration of 4×10^5 cells/mL. Then 200 μl of this solution was added to 35-mm petri plates and incubated at 37°C in 5% CO_2 for 1.5 h. Subsequently, 2 mL of growth medium was used to cover this sample and it was used for irradiation experiments.

2.3 2-D Cell Cultures

HeLa cells were cultured in DMEM supplemented with 10% fetal bovine serum (FBS), 20 IU of penicillin/mL, 20 IU of streptomycin/mL, and 0.4 mM L-glutamine at 37°C in 5% CO_2 . Cell cultures at 70% confluence were used in the irradiation experiments.

2.4 Laser Microbeam and Imaging system

The laser microbeam and imaging system was similar to a previously described setup.²⁹ An inverted microscope (Olympus iX71) was used as the experimental platform. A Nd:YAG laser (Spitlight 600, Innolas, Munich, Germany) with a pulse duration of 6 ns at $\lambda=532$ nm was used for irradiation. A combination of a $\lambda/2$ wave plate and a polarization-sensitive beamsplitter (PBS) was used to split the laser output into two beams. The beam reflected by the PBS was expanded ($2\times$), recollimated, and introduced into the back port of the microscope, wherein it was reflected upward into the back aperture of the objective by a dichroic mirror. A bright-field objective [40 \times , 0.8 numerical aperture (NA)] was used for focusing the laser beam 20 to 30 μm into the sample and also for visualization. The pulse energy was varied by introducing a linear polarizer in the path of the laser beam. Laser pulse energy at the microscope was measured by removing the objective from the turret and allowing the beam to illuminate an energy detector (J3-05, Molectron, Santa Clara, California). We used this indirect method because the large divergence angle of laser light exiting the objective made light collection difficult postobjective. The manufacturer specified transmission of our objective at 532 nm is $>90\%$. The plasma threshold (defined

as the 50% probability of generating plasma) was measured to be 6 to 7 μJ , similar to the value reported earlier.²⁹

Time-resolved imaging was done by using ultrashort illumination pulses and an intensified CCD camera. At nanosecond time delays (<100 ns) the Nd:YAG laser beam transmitted by the PBS was used to pump a dye solution to excite fluorescence. The fluorescent emission of the dye (LDS 698, Exciton) provided illumination at $\lambda=698 \pm 20$ nm with full width at half maximum duration of 15 ns. The dye fluorescence was focused by a 10 \times objective into a multimode optical fiber (400 μm diameter, Thor Labs) with the fiber distal end being placed directly onto the sample. A small water drop placed on the fiber end enabled focusing of the illumination pulse into the sample. Adjustment of the fiber length by using different fiber optic lines provided the desired time delay between delivery of the pulsed laser microbeam to the target and illumination for imaging. At time delays >100 ns, an ultrashort flash lamp, that was externally triggered by an intensified CCD (ICCD) camera (Andor iStar) was used to provide illumination. The flash lamp (KL-L, High Speed Photo Systeme, Germany) provides a broad spectral output ($\lambda=400$ to 700 nm) with a flash duration of 40 ns (FWHM). The flash lamp output was coupled into a 10 \times objective that was focused onto the sample. The ICCD was mounted on the microscope side port and triggered electronically from the laser Q-switch with a rise time of <1 ns. We used a camera gate duration of 10 ns for the fiber optic illumination and a gate duration of 100 ns for the flash lamp illumination.

2.5 Confocal Fluorescence Microscopy

2.5.1 Corneal epithelium and stroma

All fluorescent assays were on done on freshly prepared rat cornea. Cell viability was assessed using propidium iodide (PI) and cell morphology by staining actin with fluorescently labeled phalloidin in whole tissue. After laser irradiation, the cornea was incubated for 20 to 30 min in minimal media containing PI (8 $\mu\text{L}/\text{mL}$). The sample was then fixed with 4% paraformaldehyde (PF) for 1 h, permeabilized for 45 min using Igepal (0.37% in PBS) and actin cytoskeleton was stained with fluorescently labeled phalloidin (Molecular Probes) for 45 min (1:50 dilution in PBS). In some cases, tissues were processed for cryosectioning by 8-h fixation in PF and overnight incubation in 30% sucrose. Tissue slices 25 to 30 μm thick were cut using a cryotome (Leica CM 1850) and stained for fluorescence microscopy as already indicated.

2.5.2 2-D and 3-D cultures

HeLa cell monolayers or 3-D cell cultures plated in 35-mm cover slip petri dishes were fixed with 4% PF for 10 min. Fixed cultures were permeabilized with Igepal (0.37% in PBS, Sigma-Aldrich) for 15 min. Actin was stained in fixed cells using phalloidin (Alexa Fluor 488, Invitrogen Inc., 1:50 dilution). After laser pulse delivery, cell viability was assessed by staining with calcein-AM (1:200 dilution in PBS) and PI (2 μmL in PBS) for 15 min.

Fluorescent images were acquired by Olympus Confocal FV1000, Zeiss LSM Meta 510 confocal and TE2000 U Nikon epifluorescent microscopes. Excitation for second-harmonic generation (SHG) in collagen was achieved using a Ti:sapphire laser (Tsunami, Coherent Inc.) (180 fs, 80 MHz) at a

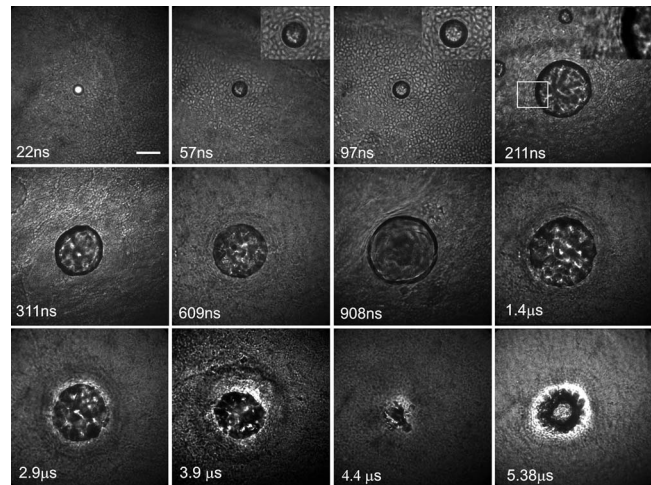


Fig. 1 Time-resolved images of laser-induced cavitation in the corneal epithelium. Insets at time points of 57, 97, and 211 ns show magnified fields around the expanding bubble, so that compressed cells can be clearly visualized. Scale bar=50 μm .

wavelength of 800 nm (40 \times , 1.3 NA objective), and emission was collected in backscattered geometry. A bandpass filter in the wavelength range of 390 to 460 nm was placed in front of the photomultiplier tube to block IR radiation. Image processing was done with Adobe Photoshop (Adobe Systems) and Metamorph (Universal Imaging Corporation) softwares. In all images, brightness and contrast were adjusted using the levels menu in Adobe Photoshop.

3 Results

3.1 Corneal Epithelium

Cavitation-induced damage was studied *ex vivo* samples of rat corneas in the epithelium and stroma. Figure 1 shows results of time-resolved imaging for laser pulses focused into the corneal epithelium at a pulse energy of 21 μJ ($3\times$ the plasma threshold). We mainly chose this energy to be consistent with earlier studies on laser induced cell lysis in 2-D cultures.²⁹ The laser-generated plasma devolves into a cavitation bubble within 30 ns of the laser pulse delivery. The rapid bubble expansion results in rupture of the epithelium that can be observed through the bubble. During expansion, we can observe severe compression of cells at the bubble rim, while cells in the next layer appear to be unaffected (inset at time points 57, 97, and 211 ns). As the bubble grows larger in size, two to three cell layers beyond the bubble are compressed (609 ns, 1.4 and 2.9 μs time points). The compression of these cell layers probably caused a change in refractive index, enabling us to visualize the border of this zone. The bubble maximum radius of 75 μm was reached <1 μs at this pulse energy. During bubble collapse, we observed recoil, only on a few occasions. The compressed cell layers also appeared to relax back since we could not see the “zone of compression” during the collapse phase (4.4 μs time point). After the final collapse, sometimes a small bubble persisted at the site for a few seconds.

Due to the rapid dispersion of the shock wave in tissue we could not image the shock wave at a pulse energy of 21 μJ

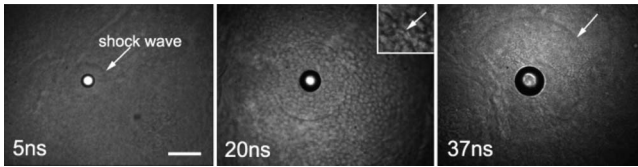


Fig. 2 Time-resolved imaging of shock wave radiation in the corneal epithelium. Arrows indicate the propagating edge of the shock wave. The shock wave does not cause any cell deformation (clearly seen in the inset at the 20-ns time point). Scale bar=50 μm .

(Fig. 1). To observe shock wave interactions within the corneal epithelium, we irradiated these samples with a pulse energy of 40 μJ (Fig. 2). As seen in Fig. 2, the shock wave radiated outward into the tissue and did not result in any displacement or deformation of the cells. This confirms earlier observations of laser-induced cell lysis in adherent cell cultures, where the shock wave was also observed not to contribute to cell lysis.²⁹

3.2 Corneal Stroma

Time-resolved studies of cavitation-induced damage in the stroma are shown in Fig. 3. The cavitation bubble expansion was damped by the dense collagen fibers of this layer as compared to the epithelium and thus it grew to a smaller maximum radius of 59 μm . The few keratocytes near the site of bubble growth appeared to be unaffected by the expansion. The bubble growth was also not completely symmetric, as compared to the corneal epithelium. The unsymmetric expansion could be due to differences in collagen organization at different locations. The maximum bubble radius of 59 μm was attained within <2 μs , and bubble splitting could also be observed (1.955 μs time point). Instances of bubble splitting can also be observed during the bubble collapse phase. Bubble collapse occurred within 3 μs and in most cases it led to a residual cavity that slowly dissolved over a few minutes.

We also conducted ablation studies in 3-D cultures to determine the effects of the matrix on bubble dynamics (Fig. 4). The cavitation dynamics for this sample are less damped as compared to the corneal stroma with the bubble achieving a

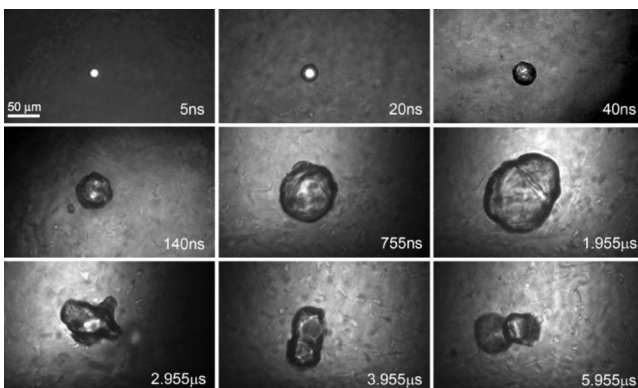


Fig. 3 Time-resolved images of laser-induced cavitation in the corneal stroma. The bubble expansion is not symmetric, with bubble splitting being observed at later time points. The dense collagen fibers cause damping of the bubble growth, reducing its maximum size. Keratocytes close to the bubble do not appear to be affected.

maximum radius of 128 μm . Bubble growth and collapse is symmetric, indicating the largely isotropic nature of the collagen gels. Certain features such as cell compression at the bubble rim (arrows at the 7.87- and 15.84- μs time points) could also be seen.

3.3 Bubble Size Quantification

To help in the comparison of the bubble dynamics in different tissue we have presented the data in a graphical form in Fig. 5. Three time-resolved images of cavitation bubble expansion in the corneal epithelium and stroma and in 3-D cultures were used to determine the average bubble size. Figure 5(a) presents results of bubble expansion for 2-D and 3-D cultures. The data for 2-D cultures are from Fig. 3 of Ref. 29. We observe that in 3-D cultures the maximum bubble radius (128 μm) is reduced due to the damping provided by the collagen matrix and the bubble collapse time is also shortened as compared to the 2-D case. These effects are heightened when we consider cavitation in the corneal epithelium and stroma [Fig. 5(b)]. The maximum bubble radius was 75 (at 0.9 μs) and 59 μm (at 1.955 μs) for the epithelium and stroma, respectively. Bubble collapse in the tissue was also significantly shorter as compared to *in vitro* samples. Bubble collapse in the epithelium occurred within <4.5 μs with considerable variations in bubble size during collapse. We did not plot bubble collapse sizes in the stroma, since the bubble did not assume a spherical shape during collapse and thus size was difficult to ascertain.

3.4 Characterization of Damage by Phase-Contrast and Fluorescence Microscopy

The site of ablation in the corneal epithelium was characterized by phase-contrast and confocal fluorescence microscopy. Figures 6(a)–6(d) present phase contrast images of control and ablated samples. In irradiated samples we observe that the top layer is peeled off, exposing this secondary layer due to the cavitation bubble expansion [Fig. 6(c)]. Cells surrounding this region and within two to three layers are compressed [Fig. 6(d)].

Confocal fluorescence microscopy of the ablated site revealed the cell morphology postablation. In Figs. 6(e)–6(h), confocal sections at different depths at the ablation site after staining actin with fluorescently labeled phalloidin revealed different cell morphologies in each epithelial layer with large flat cells at the air interface decreasing in size toward the interior. It was also observed that the diameter of the ablated site reduced deeper in the epithelial layer. The change in cell morphology could account for reduction in damage deeper into the epithelium. Cell viability was also examined by staining dead cells with PI. In Fig. 6(i) and 6(j) a top view of two ablation sites shows that PI staining is restricted to the damage site and no dead cells are observed in layers that experienced compression during cavitation bubble expansion. A cross section through an ablated region [Figs. 6(k) and 6(l)] enabled visualization of the complete damage site and showed extensive PI staining in the damage zone. The site of damage, measured to be $\approx 38 \mu\text{m}$ in radius, was smaller than the average maximum bubble size of 75 μm , indicating that the cell damage occurred within 100 ns. Cross sections at control

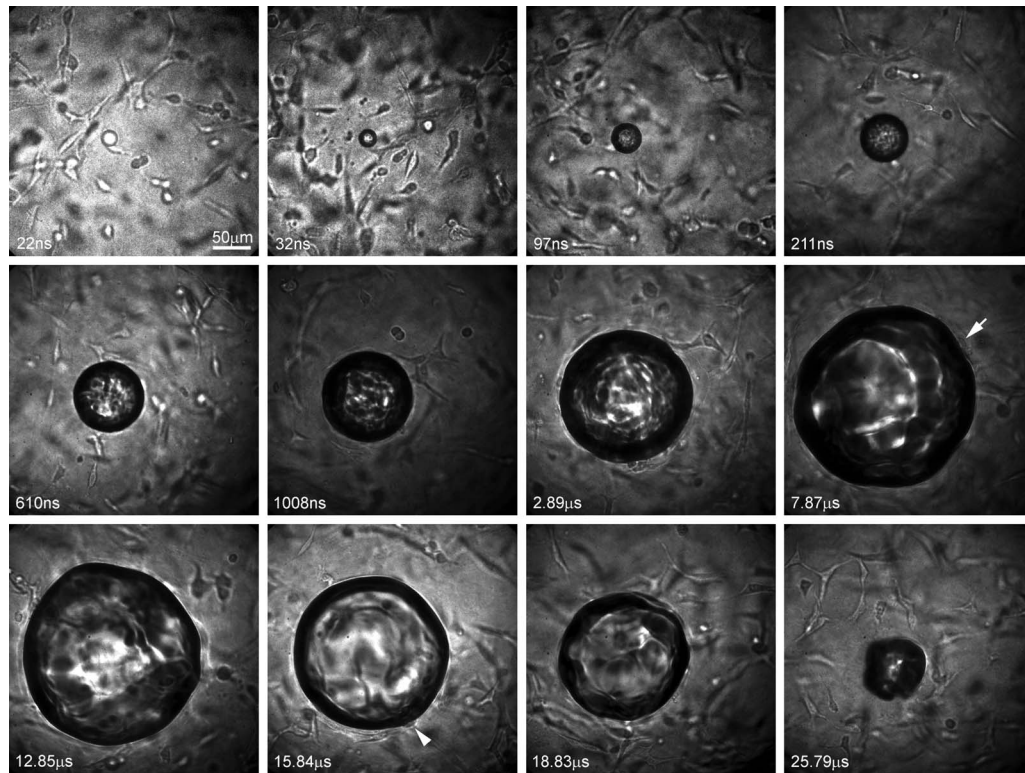


Fig. 4 Time-resolved images of laser-induced cavitation in 3-D cultures. The collagen matrix provides less damping as compared to the stroma, enabling the bubble to grow to a larger maximum size. Bubble growth and collapse are also symmetric. Cells close to the expanding bubble appear compressed, indicated by arrows at the 7.87- and 15.8- μ s time points. Scale bar=50 μ m.

sites did not show any PI staining, indicating that our sample handling protocol did not result in cell death.

Ablation effects were studied in the stroma by SHG imaging of collagen. Figure 7 presents SHG images collected at a control and ablation site in a 30- μ m horizontal section of the stroma. At the control site [Fig. 7(a)], the stroma is revealed to be comprised of regularly spaced collagen fibers as seen in earlier reports.³⁰ Keratocytes were also imaged after staining actin with fluorescently labeled phalloidin [Fig. 7(b)]. The cell morphology appeared flat and spread out with dendrites emanating at various points. At the ablation site [Fig. 7(c)], the ablated zone appears sharp, indicating rupture of collagen fibers at that point. The collagen layers around this main damage site also appear compressed due to the expanding cavitation bubble. The average radius of this ablation region in the stroma was 17 μ m, i.e., much smaller than the maximum bubble radius of 59 μ m. Keratocytes present beyond the primary damage site were ruptured, indicating the lower damage thresholds for these cells.

We also determined cell viability and cytoskeletal changes for ablation in 2-D and 3-D cultures. These results are presented in Fig. 8. In both 2-D and 3-D cultures, we observe that cells in the central region around the site of laser focus are cleared out due to stresses generated during bubble expansion [Figs. 8(a), 8(b), 8(d), and 8(e)]. However, cells experiencing large stresses at the edge of the cleared regions remain viable. The radius of the ablated zone was \approx 150 μ m in the case of 2-D cultures. The ablation zone was difficult to define for 3-D cultures due to the random arrangement of cells

within the collagen matrix. However, based on patterns of staining of live cells we measured the ablation region to be \approx 71 μ m in radius [dotted oval in Fig. 8(d)]. Staining the actin cytoskeleton enabled us to visualize the effects on cell morphology. In 2-D cultures, cells at the edge of the primary damage zone did not show any change in morphology even after being exposed to large shear stresses [Fig. 8(c)]. This cellular response appeared similar to that seen in the corneal epithelium. In 3-D cultures, we could not observe any ablated region in the collagen matrix, probably due to faster “healing” as compared to the stroma. Damage to the cell dendrites was visible, but cell rupture was not seen in any samples [Fig. 8(f)].

4 Discussion

Laser-induced damage was studied by a combination of time-resolved imaging and fluorescence microscopy in *ex vivo* samples of rat corneas. Our time-resolved imaging system enabled visualization of the cellular response to cavitation bubbles in rat corneal tissue. Note that these had not been observed before at such high spatial resolution. Studies in the corneal epithelium and stroma revealed the difference in cavitation dynamics depending upon the tissue organization. In general, the images revealed that (1) the cavitation bubble growth is significantly dampened due to the tissue matrix and cell organization as compared to *in vitro* 2-D and 3-D cultures and (2) the size of the damage zone as defined by cell viability was smaller than the maximum bubble size, indicating that

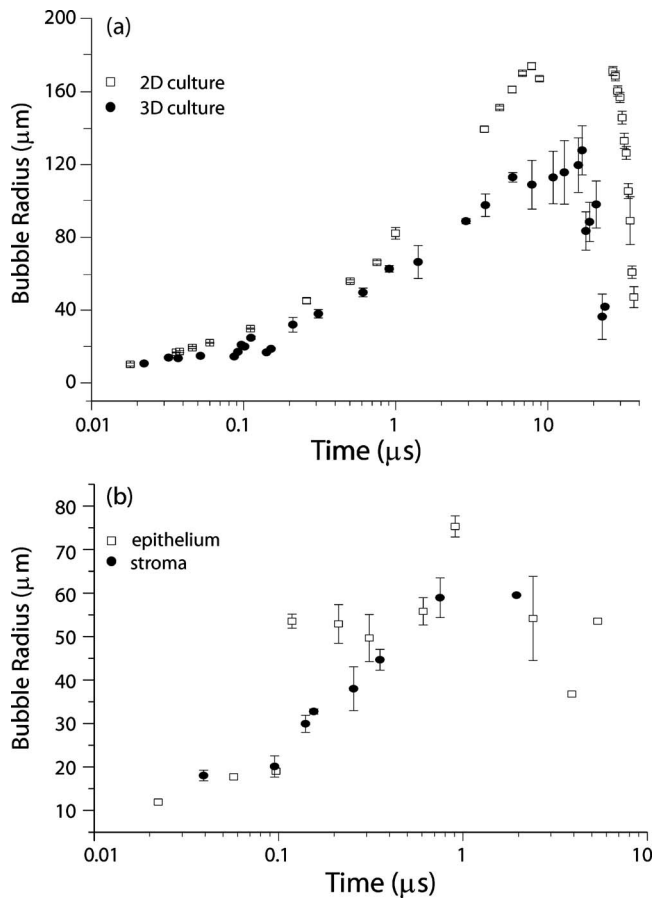


Fig. 5 Quantification of bubble growth in (a) 2-D and 3-D cultures and (b) *ex vivo* corneal epithelium and stroma. Note the different y axis scales in (a) and (b). Data for 2-D cultures are from Fig. 3 of Ref. 29.

damage occurred on nanosecond timescales. The reduction in maximum bubble radius was in the range of 54 to 59% for bubble expansion in tissue as compared to 2-D or 3-D cultures.

In the epithelium, primary damage occurred due to rapid bubble expansion and caused cell rupture and peeling of cell layers (Fig. 1). Beyond the primary damage site, cells underwent large deformations (compression) due to the expanding bubble but remained intact. This compression could extend two to three cell layers beyond the bubble rim. Such a deformation mode has not been observed in earlier studies of laser ablation of tissue. During the collapse phase these cell layers relaxed back to their original positions. At the end of collapse, we either observed a residual cavity or, in some cases, a peeled off layer of cells. In an earlier study on laser ablation of *in vitro* epithelial cell cultures it was observed that cells experiencing large fluid shear stresses (180 to 220 kPa) due to cavitation bubble expansion in the medium could remain intact and viable.²⁹ In this study, while the mode of deformation is compressive, cellular resistance to these large forces appeared to be at the same level. This indicates that cells might have a general mechanism enabling them to withstand large stresses on small timescales.

In the stroma, the layered collagen fiber organization as revealed by SHG imaging provided even more damping to the cavitation bubble than in the epithelium. Thus, the bubble expanded to a smaller maximum size (59 μm) as compared to the epithelium (75 μm). Other effects such as bubble splitting were also observed, which could be due to the specific arrangement of collagen fibers affecting the bubble growth. Keratocytes close to the site of bubble expansion appeared to be unaffected, but due to the low cell density in the stroma it was difficult to specifically note cell damage. Stromal effects already noted were further highlighted by examining cavitation dynamics in 3-D cultures. These cultures differ from the stroma in their random arrangement of collagen fibers and sparser packing of these fibers.³¹ Due to this, the cavitation bubble experienced less damping and grew symmetrically to a larger maximum size (128 μm). This indicated that the viscous damping experienced by the bubble was less than even that in the epithelium.

Recently, Brujan and Vogel produced a detailed analysis of bubble dynamics in tissue phantoms made from polyacrylamide gels (PAA) with varying mechanical properties.²⁸ They observed that optical breakdown led to the generation of a tensile wave that could also be responsible for tissue damage. The magnitude of the tensile wave was dependent on the laser pulse energy used to create cavitation bubbles. In our experiments, the effects of this tensile wave on tissue damage cannot be separated from damage due to bubble expansion. The magnitude of the tensile wave would also be extremely low due to the low pulse energies used to create optical breakdown in our studies as compared to those of Brujan and Vogel. Their study further highlighted the importance of considering the dynamic mechanical properties of the tissue since it would behave as a stiffer material at short timescales. We experimentally observe that cells do withstand considerable compressive stresses on nanosecond timescales without any physical damage. However, quantification of these stresses would be outside the purview of this study, since a detailed force analysis would be necessary.

Phase contrast and confocal fluorescence microscopy on ablated regions enabled us to determine the acute impact of laser pulses in corneal tissue. Phase-contrast imaging of damaged regions in the epithelium showed that the cavitation bubble led to rupture and peeling of the primary epithelial layers [Figs. 6(a)–6(d)]. In some cases, cells experiencing compression due to the expanding bubble retained their compressed appearance after bubble collapse. At other times we could observe the cell sheet being restored to its original shape. Whole tissue and cryopreserved tissue sections were used to determine cell viability and cytoskeletal morphology using confocal fluorescence microscopy. An interesting observation was that the size of the damage zone decreased deeper into the epithelium [Figs. 6(e)–6(h)]. Since the laser was focused into the epithelium, we expected a symmetrical damage zone in the layers above and below the site of laser focus. However, we observed that damage to the exterior epithelial layers (near the air interface) as characterized by peeling off or by the size of the cavity was always greater than to the interior layers. This indicated that the different cell layers in the epithelium had different mechanical properties. The exterior cell layers were flat and of a larger size, while the inner cell layers had smaller cuboid cells with many cell-cell junc-

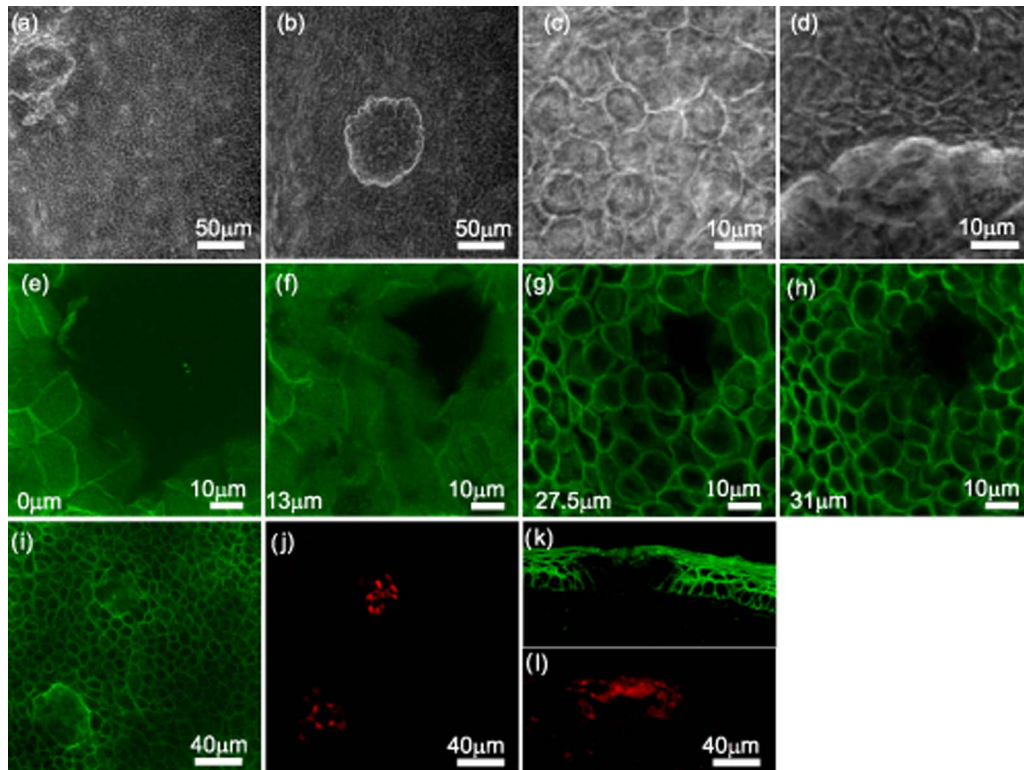


Fig. 6 Laser-induced damage in the corneal epithelium imaged by phase-contrast and confocal fluorescence microscopy. Phase-contrast images of control [(a) and (c)] and ablation sites [(b) and (d)] show that the primary layer of epithelial cells is cleared off in the ablated sample. The cell layers surrounding this damage region have a compressed appearance (d). Confocal fluorescence microscopy sections of one ablation site after staining actin with fluorescently labeled phalloidin [(e) to (h)]. The imaging depth is given in the lower left corner. The size of the ablation zone decreases deeper into the epithelium. Cell morphology is also strikingly different in different layers. (i) and (j) Top view of two ablated sites. Fluorescently labeled phalloidin marked the actin cytoskeleton (i) and dead cells were marked with propidium iodide (j). The ablated region seen by PI staining is smaller than the maximum bubble diameter in the epithelium. (k) and (l) Cross sections of ablated corneal samples enable visualization of the different epithelial layers using actin staining with phalloidin (k). In the ablated region, dead cells are stained with PI (l), providing a measure of its size. Cells two layers away from the primary ablation site are also stained with PI, indicating that these layers are also affected due to the cavitation bubble expansion.

tions. The tighter packing of the inner cell layers may have contributed to their resilience. Also, the collagenous stroma might offer some damping to the inner cell layers accounting for their lower damage potential. The actin cytoskeleton of the cells neighboring the ablation site did not show any disruption. This was surprising given the large deformations that these cells were subject to during cavitation bubble expansion. Further, we observed cell death only adjacent to the site of laser focus and the size of the ablated region was much reduced compared to the average maximum bubble size (38 versus $75 \mu\text{m}$, respectively) [Fig. 6(i)]. This was also clearly seen in tissue cross sections, where cellular disruption and cell death was localized to a small region [Figs. 6(j) and 6(k)].

In the stroma, we could observe the collagen structure by using the intrinsic second-harmonic signal. Examining the control site, we see that the stroma is a laminate structure with flattened keratocytes occurring in layers between the collagen fibers³² [Figs. 7(a) and 7(b)]. Laser ablation in the stroma resulted in a damage zone with sharp edges due to collagen fiber rupture [Fig. 7(c)]. Again, the size (radius) of the damage region was smaller than the maximum bubble radius (17 versus $59 \mu\text{m}$). Keratocytes present around this ablation zone were completely cleared out with only partial cell remains

being seen [Fig. 7(d), arrows]. This is expected given the large difference in mechanical properties of keratocytes ($E = 1$ to 10 kPa) and collagen ($E = 1$ to 3 GPa).³³ Moreover, although it is known that keratocytes are mechanically attached to collagen this does not appear to provide any buffering to these cells.³⁴

These cellular responses are further highlighted if we consider the ablation characteristics in 2-D and 3-D cultures (Fig. 8). Cavitation damage in confluent HeLa cell monolayers was seen to produce a circular zone that was cleared of cells. The size of this damage zone ($150 \mu\text{m}$) was much larger than in the corneal epithelium. (Note that the ablated region for HeLa cells was much larger than observed in the earlier report on laser-induced damage in PtK₂ cells.²⁹ We believe this difference could be due to cell type and the nature of cell-substrate and cell-cell adhesion). Since the cavitation bubble attains a larger maximum size in culture medium²⁹ ($180 \mu\text{m}$) as compared to the cornea ($75 \mu\text{m}$), the damage potential is also higher. Cytoskeletal morphology of HeLa cells and the outer layers of the corneal epithelium appeared similar, characterized by dense actin bonds at the edge of large flattened cells. Similar to HeLa cells, the corneal epithelial cells in the outer

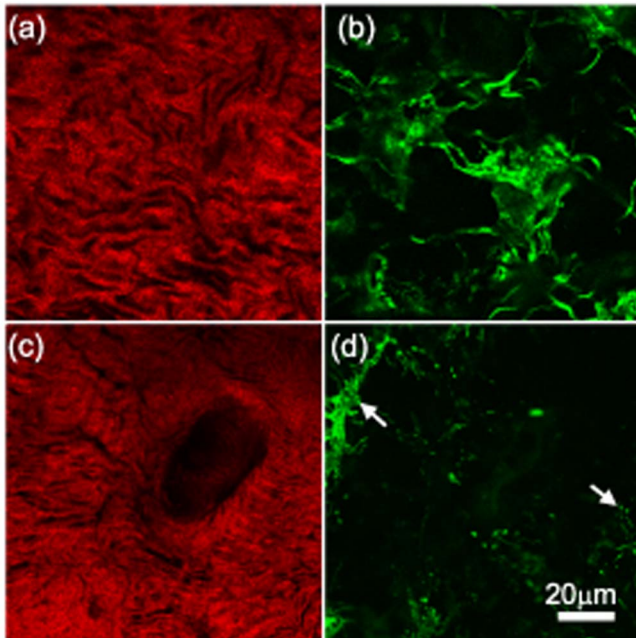


Fig. 7 Second-harmonic imaging microscopy of collagen organization and confocal microscopy of keratocytes in the stroma: (a) control area with regular collagen organization observed by SHG; (b) keratocyte actin visualized with fluorescently labeled phalloidin; (c) at an ablation site collagen fibers exhibit a clean edge, indicating fiber rupture; and (d) keratocytes beyond the primary damage site are ablated leaving behind cellular debris [arrows in (d)].

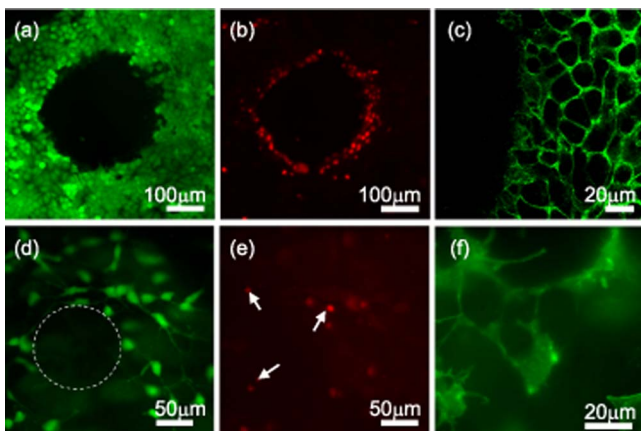


Fig. 8 Laser-induced damage in 2-D and 3-D cultures imaged by epifluorescence imaging. (a) and (b) Images showing viability of HeLa cells at an ablation site 30 min postirradiation. Calcein AM stains viable cells (a) while PI stains dead cells (b). A central area around the site of laser focus is completely cleared of cells. Cells at the periphery of the damage zone are viable, while cells beyond it are dead. In 3-D cultures [(d) and (e)], cells away from the irradiation site show no change (d), while cells at the periphery of the damage site are dead [arrows in (e)]. The dotted oval in (d) marks the ablation zone observed in 3-D cultures. In (c), actin staining with phalloidin of HeLa cells at the edge of the damage site shows these cells to be unaffected, similar to observations in the corneal epithelium. In (f), actin staining near the irradiation site in 3-D cultures shows minimal damage to these cells.

layer also exhibited an increased propensity to cavitation damage as compared to the inner layers. This lowered resistance to cavitation damage could be due to less number of cell-cell contacts, indicating that this might be a major determinant of cell survival to cavitation forces. In both cases (epithelium and 2-D cultures), the cells that did survive the cavitation-induced stress showed little disruption of actin cytoskeleton. Thus, the main difference between the cellular response in 2-D cultures and epithelial tissue is the significant reduction in primary damage in tissue due to the resistance offered to bubble growth. Cells surviving deformation due to bubble expansion show morphology similar to control cells, indicating that cellular resistance might be due to factors other than the actin network. A likely possibility is that the intermediate filament network maybe responsible for absorbing the cavitation-induced stress. Intermediate filaments have lower stiffness and are known to be involved in controlling cell morphology during exposure to shear stress.³⁵ Comparing 3-D cultures to the stromal response, we see that the damage zone in 3-D cultures (shown by PI staining) was larger (71 versus 17 μm). Collagen fibers in 3-D cultures are not regularly stacked as in the stroma, nor is the density as high.³¹ Furthermore, the bubble grew to a maximum radius that was much larger in 3-D cultures (128 μm) compared to the stroma (59 μm), indicating that the collagen did not provide much damping in 3-D cultures. These factors contributed to the higher cell damage seen in 3-D cultures as compared to the stroma. The cell morphology in 3-D cultures was also different compared to the stroma since fibroblasts were not stacked in ordered layers like in the stroma. Therefore, we believe that comparing results between 3-D cultures and stroma would not be valid, and also sound a cautionary note for the use of these 3-D cultures as tissue equivalents.

Finally, our results could also be of interest to the study of ultrasound-mediated drug delivery. As shown by our experiments, it is possible to image cavitation effects in tissue to determine cellular response. In ultrasound drug delivery, multiple cavitation bubbles are produced that expand and collapse on similar timescales to produce tissue damage and permeabilization. The range of cavitation damage and the cellular response have not been imaged on nanosecond timescales and our system provides a method to accomplish that. Combined with fluorescence microscopy it could provide insights into the role of cavitation bubbles in achieving transdermal drug delivery.

5 Conclusions

Pulsed laser ablation of corneal epithelium and stroma was studied by time-resolved imaging and confocal fluorescence microscopy. Time-resolved imaging provided cellular level resolution of bubble dynamics in these tissue, enabling characterization of the response of cells to bubble expansion. Bubble expansion was strongly damped in tissue as compared to 2-D and 3-D *in vitro* cultures with a bubble size reduction in the range of 54 to 59% in tissue. Cell damage zones (radii) were much reduced as compared to the maximum bubble size. Specifically, they were 38 and 17 μm as compared to maximum bubble sizes of 75 and 59 μm in the epithelium and stroma, respectively. Cells could withstand significant deformation without loss of viability or change in the actin cytosk-

leton. Bubble expansion led to epithelial sheet rupture and compression of cells in neighboring layers, with these cells surviving this deformation without any visible damage. In the stroma, keratocytes exhibited higher damage potential as compared to collagen fibers. Comparison with 2-D and 3-D cultures indicated that while ablation in 2-D cultures gave responses similar to the corneal epithelium, 3-D cultures were not representative of the stroma. For 3-D cultures, the damage zone radius ($71\ \mu\text{m}$) was much larger as compared to the stroma due to the nonspecific arrangement of collagen fibers in these samples. Our results thus provide a comprehensive description of physical and acute biological effects of nanosecond laser pulses in the cornea.

Acknowledgments

KRR thanks Vasan Venugopalan and Nancy Allbritton for encouragement and valuable discussions. We acknowledge support from the National Institutes of Health (USA) via the Fogarty International Research Collaboration Award No. 1 RO3-TW007323-01. We acknowledge the Wellcome Trust, United Kingdom (NLO-056727/Z/99/B) and the Department of Science and Technology, Government of India, Centre for Nanotechnology (No. SR/S5/NM-36/2005), and the NCBS imaging facility for use of the Zeiss LSM 510 metaconfocal microscope and Olympus FV1000 confocal microscope, respectively.

References

1. A. Vogel and V. Venugopalan, "Mechanisms of pulsed laser ablation of biological tissue," *Chem. Rev. (Washington, D.C.)* **103**, 577–644 (2003).
2. R. F. Steinert and C. A. Puliafito, *The Nd:YAG Laser in Ophthalmology: Principles and Clinical Applications of Photodisruption*, W. B. Saunders, Philadelphia (1985).
3. F. H. Loesel, M. H. Niemz, J. F. Bille, and T. Juhasz, "Laser-induced optical breakdown on hard and soft tissues and its dependence on the pulse duration: experiment and model," *IEEE J. Quantum Electron.* **32**(10), 1717–1722 (1996).
4. A. Vogel, J. Noack, G. Hüttman, and G. Paltauf, "Mechanisms of femtosecond laser nanosurgery of cells and tissues," *Appl. Phys. B* **81**(8), 1015–1047 (2005).
5. J. Colombelli, S. W. Grill, and E. H. K. Stelzer, "Ultraviolet diffraction limited nanosurgery of live biological tissues," *Rev. Sci. Instrum.* **75**(2), 472–478 (2004).
6. G. D. Meredith, C. E. Sims, J. S. Soughayer, and N. L. Allbritton, "Measurement of kinase activation in single mammalian cells," *Nat. Biotechnol.* **18**(3), 309–312 (2000).
7. K. Schütze and G. Lahr, "Identification of expressed genes by laser-mediated manipulation of single cells," *Nat. Biotechnol.* **16**(8), 737–742 (1998).
8. S. Thalhammer, G. Lahr, A. Clement-Sengewald, W. M. Heckl, R. Burgemeister, and K. Schütze, "Laser microtools in cell biology and molecular medicine," *Laser Phys.* **13**(5), 681–691 (2003).
9. J. F. Fujimoto, W. Z. Lin, E. P. Ippen, C. A. Puliafito, and R. F. Steinert, "Time-resolved studies of Nd:YAG laser-induced breakdown: plasma formation, acoustic wave generation, and cavitation," *Invest. Ophthalmol. Visual Sci.* **26**(12), 1771–1777 (1985).
10. A. Vogel, S. Busch, and U. Parlitz, "Shock wave emission and cavitation bubble generation by picosecond and nanosecond optical breakdown in water," *J. Acoust. Soc. Am.* **100**(1) 148–165 (1996).
11. A. Vogel, K. Nahen, D. Theisen, and J. Noack, "Plasma formation in water by picosecond and nanosecond Nd:YAG laser pulses—Part I: optical breakdown at threshold and superthreshold irradiance," *IEEE J. Sel. Top. Quantum Electron.* **2**(4), 847–860 (1996).
12. T. Kodama and Y. Tomita, "Cavitation bubble behavior and bubble-shock wave interaction near a gelatin surface as a study of in vivo dynamics," *Appl. Phys. B* **70**(1), 139–149 (2000).
13. E.-A. Brujan, K. Nahen, P. Schmidt, and A. Vogel, "Dynamics of laser-induced cavitation bubbles near an elastic boundary," *J. Fluid Mech.* **433**, 251–281 (2001).
14. E.-A. Brujan, K. Nahen, P. Schmidt, and A. Vogel, "Dynamics of laser-induced cavitation bubbles near elastic boundaries: influence of the elastic modulus," *J. Fluid Mech.* **433**, 283–308 (2001).
15. T. Juhasz, X. H. Hu, T. Laszlo, and Z. Bor, "Dynamics of shock waves and cavitation bubbles generated by picosecond laser pulses in corneal tissue and water," *Lasers Surg. Med.* **15**(1), 91–98 (1994).
16. T. Juhasz, G. A. Kastis, C. Suárez, Z. Bor, and W. E. Bron, "Time-resolved observations of shock waves and cavitation bubbles generated by femtosecond laser pulses in corneal tissue and water," *Lasers Surg. Med.* **19**(1), 23–31 (1996).
17. A. Vogel, P. Schweiger, A. Frieser, M. N. Asiyu, and R. Birngruber, "Intraocular Nd:YAG laser surgery: light-tissue interaction, damage range and reduction of collateral effects," *IEEE J. Quantum Electron.* **26**(12), 2240–2260 (1990).
18. A. Vogel, M. R. C. Capon, M. N. Asiyu-Vogel, and R. Birngruber, "Intraocular photodisruption with picosecond and nanosecond laser pulses: Tissue effects in cornea, lens, and retina," *Invest. Ophthalmol. Visual Sci.* **35**(7), 3032–3044 (1994).
19. A. Vogel, S. Busch, K. Jungnickel, and R. Birngruber, "Mechanisms of intraocular photodisruption with picosecond and nanosecond laser pulses," *Lasers Surg. Med.* **15**(1), 32–43 (1994).
20. F. H. Loesel, J. P. Fischer, M. H. Götz, C. Horvath, T. Juhasz, F. Noack, N. Suhm, and J. F. Bille, "Non-thermal ablation of neural tissue with femtosecond laser pulses," *Appl. Phys. B* **66**(1), 121–128 (1998).
21. H. Lubatschowski, G. Maatz, A. Heisterkamp, U. Hetzel, W. Drommer, H. Welling, and W. Ertmer, "Application of ultrashort laser pulses for intrastromal refractive surgery," *Graefes Arch. Clin. Exp. Ophthalmol.* **238**(1), 33–39 (2000).
22. G. Maatz, A. Heisterkamp, H. Lubatschowski, S. Barcikowski, C. Fallnich, H. Welling, and W. Ertmer, "Chemical and physical side effects at application of ultrashort laser pulses for intrastromal refractive surgery," *J. Opt. A, Pure Appl. Opt.* **2**(1), 59–64 (2000).
23. A. Heisterkamp, T. Mamom, O. Kermani, W. Drommer, H. Welling, W. Ertmer, and H. Lubatschowski, "Intrastromal refractive surgery with ultrashort laser pulses: in vivo study on the rabbit eye," *Graefes Arch. Clin. Exp. Ophthalmol.* **241**(6), 511–517 (2003).
24. S. E. Wilson, R. R. Mohan, J.-W. Hong, J.-S. Lee, R. Choi, and R. R. Mohan, "The wound healing response after laser in situ keratomileusis and photorefractive keratectomy," *Arch. Ophthalmol. (Chicago)* **119**, 889–896 (2002).
25. W. J. K. Langenbeck, S. Schründer, E. P. Zhang, and F. Hoffmann, "Immunohistology of corneal wound healing after photorefractive keratectomy and laser in situ keratomileusis," *J. Refract. Surg.* **15**(4) 451–458 (1999).
26. S. Toyran, Y. Liu, S. Singha, S. Shan, M. R. Cho, R. J. Gordon, and D. P. Edward, "Femtosecond laser photodisruption of human trabecular meshwork: an in vitro study," *Exp. Eye Res.* **81**(3), 298–305 (2005).
27. C. Meltendorf, G. J. Burbach, J. Bühren, R. Bug, C. Ohrloff, and T. Deller, "Corneal femtosecond laser keratotomy results in isolated stromal injury and favorable wound-healing response," *Invest. Ophthalmol. Visual Sci.* **48**, 2068–2075 (2007).
28. E.-A. Brujan and A. Vogel, "Stress wave emission and cavitation bubble dynamics by nanosecond optical breakdown in a tissue phantom," *J. Fluid Mech.* **558**, 281–308 (2006).
29. K. R. Rau, P. A. Quinto-Su, A. N. Hellman, and V. Venugopalan, "Pulsed laser microbeam-induced cell lysis: time-resolved imaging and analysis of hydrodynamic effects," *Biophys. J.* **91**(1), 317–329 (2006).
30. M. Han, G. Giesec, and J. F. Bille, "Second harmonic generation imaging of collagen fibrils in cornea and sclera," *Opt. Express* **13**(15), 5791–5797 (2005).
31. A. Zoumi, A. Yeh, and B. J. Tromberg, "Imaging cells and extracellular matrix in vivo using second-harmonic generation and two-photon excited fluorescence," *Proc. Natl. Acad. Sci. U.S.A.* **99**(17), 11014–11019 (2002).
32. J. V. Jester, P. A. Barry, G. J. Lind, W. M. Petroll, R. Garana, and H. D. Cavanagh, "Corneal keratocytes: in situ and in vitro organization of cytoskeletal contractile proteins," *Invest. Ophthalmol. Visual Sci.*

- 35(2), 730–743 (1994).
33. J. L. Alonso and W. H. Goldmann, “Feeling the forces: atomic force microscopy in cell biology,” *Life Sci.* **72**, 2553–2560 (2003).
34. L. J. Müller, L. Pels, and G. F. J. M. Vrense, “Novel aspects of the ultrastructural organization of human corneal keratocytes,” *Invest. Ophthalmol. Visual Sci.* **36**(13), 2557–2567 (1995).
35. B. P. Helmke, D. B. Thakker, R. D. Goldman, and P. F. Davies, “Spatiotemporal analysis of flow-induced intermediate filament displacement in living endothelial cells,” *Biophys. J.* **80**(1), 184–194 (2001).